Research Article | Vol. 28, No. 18 / 31 August 2020 / Optics Express 26161
Optics EXPRESS

Proposal for a photoacoustic ultrasonic generator based on Tamm plasmon structures

ELIZAVETA I. GIRSHOVA,[1,*] ALENA P. MIKITCHUK,[2] ALEXEY V. BELONOVSKI,[3] KONSTANTIN M. MOROZOV,[1] KONSTANTIN A. IVANOV,[3] GALIA POZINA,[4] KONSTANTIN V. KOZADAEV,[2] ANTON YU. EGOROV,[3] AND MIKHAIL A. KALITEEVSKI[1,3]

[1]*St. Petersburg Academic University, 194021 St. Petersburg, Russia*
[2]*Belarusian State University, Niezaliezhnasci Avenue 4, 220030 Minsk, Belarus*
[3]*ITMO University, Kronverksky Pr. 49, 197101 St. Petersburg, Russia*
[4]*Department of Physics, Chemistry and Biology (IFM), Linköping University, SE-58183 Linköping, Sweden*
[*]*ilinishna@gmail.com*

Abstract: The scheme of a generation of ultrasound waves based on optically excited Tamm plasmon structures is proposed. It is shown that Tamm plasmon structures can provide total absorption of a laser pulse with arbitrary wavelength in a metallic layer providing the possibility of the use of an infrared semiconductor laser for the excitation of ultrasound waves. Laser pulse absorption, heat transfer and dynamical properties of the structure are modeled, and the optimal design of the structure is found. It is demonstrated that the Tamm plasmon-based photoacoustic generator can emit ultrasound waves in the frequency band up to 100 MHz with predefined frequency spectrum.

1. Introduction

Ultrasound waves are widely used for ultrasonic non-destructive evaluation, structure health monitoring, material characterization [1], orientation imaging microscopy [2] and acoustic microscopy [3,4] and optoacoustic tomography [5]. Existing conventional approach for generation of ultrasound waves utilize piezoelectric transducers, which bring some drawbacks associated with poor survivability in harsh environment, bulky size and weight, complexity of setups, high cost and susceptibility to electromagnetic interference [1]. Additionally, piezoelectric transducers exhibit a spectrum centered at the resonance frequency [6]. In contrary, photoacoustic transducers are a very attractive alternative for generation of ultrasound, because they are based on the effect of expansion of the optical absorbing layer heated by laser pulses [7,8]. In photoacoustic transducers, the absorber is heated and cooled, leading to mechanical deformations, which cause cycles of pressure, or, in the other words, acoustic waves in ambient surrounding [9]. The operation principle provides the number of advantages: reliability, compactness, full galvanic isolation [10], wideband operation [11], and possibility of realization of transducer at the edge of the optical fiber [12], that, in turn, leads to the immunity to harsh environment and electromagnetic interference. At the same time, further miniaturization, predefined spectrum of ultrasound as well as the increase of functional flexibility of the ultrasound generation is required. Such goals can be achieved by the application of plasmonic structures, especially the Tamm plasmon (TP) structures [13,14].

TP is the state of electromagnetic field localized at the interface between metal and the Bragg reflector (BR). TP structures provide a wide range of opportunities for electromagnetic mode engineering [15,16] and, in particular, for the control of the absorption of light [17]. In optoelectronic devices, absorption of light in metals is the enemy of high performance, but for

#400639 https://doi.org/10.1364/OE.400639
Journal © 2020 Received 2 Jul 2020; revised 30 Jul 2020; accepted 31 Jul 2020; published 20 Aug 2020

Optics EXPRESS

photoacoustic generators, high performance of the device is based on controllable absorption of light.

In existing photoacoustic systems, the laser wavelength usually corresponds to green-blue visible range that limits the range of possible laser systems. The use of TP structures gives opportunity to provide a total absorption in the infrared band. In this case, GaAs-based semiconductor lasers emitting at a wavelength of 980 nm can be used. Such lasers combine affordability, high power, scalability, and possibility of a direct temporal modulation of the intensity for the frequencies up to few GHz [18,19]. Semiconductor lasers operating at the wavelength of 980 nm can produce an average power of 1 W focused on the 10 μm x 10 μm spot providing a flux density up to 10^6 W/cm^2.

This paper aims to introduce the novel scheme of the photoacoustic generator based on the Tamm plasmon structure (PAG-TP) and the optimisation of its performance.

2. Design of the structure

In the proposed scheme the metallic layer of the TP structure is heated by a short laser pulse, expands and emits ultrasound waves, as shown in Fig. 1. Utilisation of the TP enhances the absorption of light in a predefined point of the structure and could improve the performance of the photoacoustic generator of ultrasound waves.

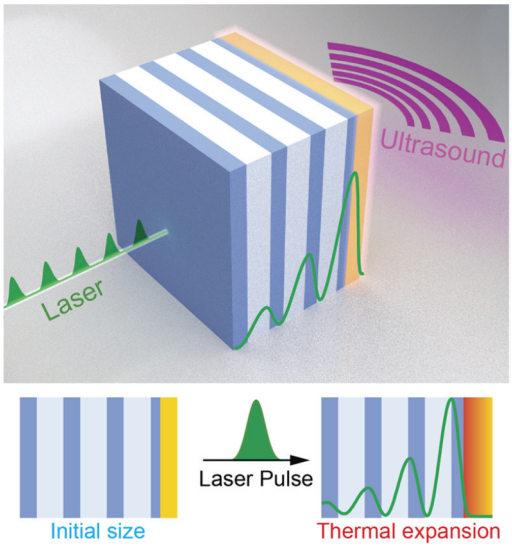

Fig. 1. Scheme of the PAG-TP structure and the principle of operation.

The structure consists of BR covered by a layer of metal and is illuminated from the BR side by the laser beam periodically modulated in time. The design of the TP structure ensures the total absorption of laser radiation at a desirable wavelength resulting in a periodic in time heating and cooling of the metallic layer. Therefore, its periodic expansion and shrinking will lead to emission of sound.

The design of the structure and the choice of the material should simultaneously provide: (i) total absorption of laser radiation at the desired wavelength; (ii) effective heating of the metallic layer by laser pulses; (iii) effective heat sink from the metallic layer in order to avoid overheating; (iv) maximal amplitude and desirable temporal shape of oscillation of the sample surface.

Optics EXPRESS

3. Results and discussion

When the layer of the material with thermal expansion coefficient ε absorbs the laser pulse with energy density G, the thickness of the layer is increased by the value B defined by

$$B = \varepsilon G/(c\rho), \tag{1}$$

where c and ρ are the specific heat capacity and density of the material, respectively. In the case of a harmonic oscillation of the surface with amplitude of oscillation B and frequency f the intensity of sound J reads as [20,21,22]:

$$J = \frac{\rho_m v}{2}(2\pi f B)^2, \tag{2}$$

where ρ_m and v are the density and speed of sound for the media, where ultrasound is emitted. Corresponding pressure, induced by of the acoustic wave P reads

$$P = 2\pi f \rho_m v B. \tag{3}$$

The efficiency of conversion of laser radiation to ultrasound waves η can be estimated as

$$\eta = \frac{J}{Gf} = 2\pi^2 \rho_m v \left(\frac{\varepsilon}{c\rho}\right)^2 Gf \tag{4}$$

As shown by Eq. (4), the key parameter defining the efficiency η is the ratio $\varepsilon/(c\rho)$ for the metal forming a top layer of the structure. Usually, metals like gold, silver or copper are used to fabricate photoacoustic emitters but as can be seen from Table 1, lithium (Li) possesses maximal value of $\varepsilon/(c\rho)$ followed by lead (Pb) and magnesium (Mg). Magnesium possesses a larger thermal diffusivity coefficient than lithium or lead. Therefore, magnesium (or its alloys) is the most suitable material for metallic layer in PAG-TP. For the materials forming the Bragg reflector, it is convenient to choose TiO_2 as the high refractive index material with large thermal diffusivity coefficient, and SiO_2 as the low refractive index materials.

Table 1. Specific heat capacity *c*, thermal conductivity κ, density ρ, thermal diffusivity D, thermal expansion coefficient ε, quantity $\frac{\varepsilon}{c\rho}$, and complex refractive index at the wavelength 980 nm for the materials used to construct TP structure.

	c $\frac{J}{kg*K}$	κ $\frac{W}{m*K}$	ρ $\frac{kg}{m^3} * 10^3$	$c\rho$ $\frac{J}{K*m^3} * 10^6$	D $\frac{m^2}{c} * 10^{-6}$	ε $\frac{10^{-6}}{K}$	$\frac{\varepsilon}{c\rho}$ $\frac{10^{12}*m^3}{J}$	$Re(n)$	$Im(n)$
Au	128	317	19.3	2.48	127	14.2	5.7	0.22	6.32
Ag	235	235	10.4	2.45	96.15	19.5	7.9	0.04	6.96
Al	897	236	10.3	2.43	97	22	9.4	1.47	9.22
Li	3390	84.7	0,534	1.8	47.7	46	25	0.22	4.96
Mg	103	156	1.73	1.78	88	25	15	1.61	9.76
Cu	385	401	8.92	3.44	116	16.6	4.0	0.32	6.45
Pb	130	35.3	11.3	1.45	30	28	19	1.37	5.14
SiO_2	772	1.38	2.2	1.698	0.812	0.5	0.29	1.45	$<10^{-4}$
TiO_2	850	12.6	4.26	3.032	4.15	9.19	3.03	2.49	$<10^{-12}$
Al_2O_3	850	30	3.99	3.3915	8.84	8.1	2.38	1.76	$<10^{-4}$

Table 1 shows the properties of some metals and dielectric materials [23–27], which can be used to construct PAG-TP. Figure 2(a) shows the detailed scheme of the TP structure, which consists of a magnesium film deposited on top of the Bragg reflector made of 4 pairs of SiO_2 and

Optics EXPRESS

TiO_2 layers with a thickness of 168 nm and 118 nm, respectively. The thickness of the layer of TiO_2 adjacent to the magnesium layer is reduced to 100 nm in order to shift the TP to the center of the stopband of the Bragg reflector and provide better localization of light. The thickness of the magnesium layer is d_M = 1000 nm.

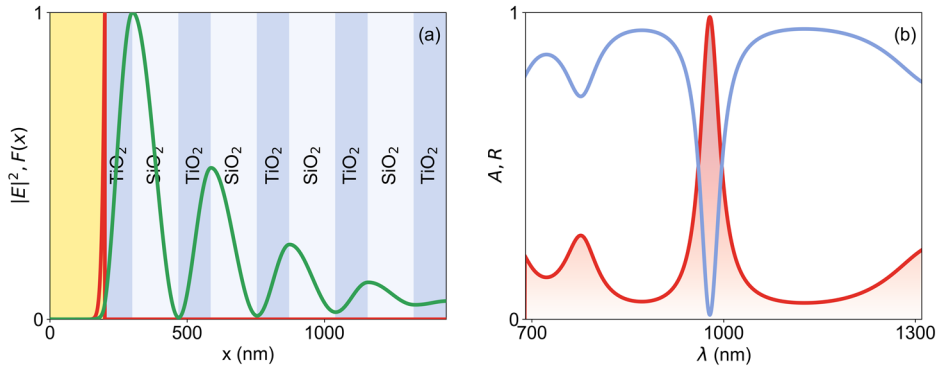

Fig. 2. (a) Scheme of the TP structure. Profile of $|E(x)|^2$ established in the TP structure under illumination by the laser with wavelength of 980 nm (green line) and the corresponding heating density (red line). (b) Absorption (red) and reflection (blue) spectra of the TP structure under illumination from BR side at normal incidence.

Spectra of absorption $A(\lambda)$ and reflection $R(\lambda)$ coefficients at normal incidence of the TP structure are shown in Fig. 2(b). The reflection and absorption spectra, and the spatial distribution of electromagnetic field in the structure were obtained by solving Maxwell's equations by means of transfer matrix method [28] (see Supplementary Supplement 1). Clearly, there is a sharp peak of absorption at the wavelength of 980 nm corresponding to the TP resonance, with the maximum value being close to unity. Note that when the light is incident on the interface of magnesium from the uniform material, the reflection coefficient at the wavelength of 980 nm is ~0.8. The green line in Fig. 2(a) shows the spatial profile of $|E(x)|^2$, where $E(x)$ is electric field established within the structure under illumination by the light with wavelength of 980 nm. It can be seen that the electric field is localized near the interface of the metal and the penetration depth is $\xi \approx 15$ nm.

The total intensity absorbed by the structure is equal to the product of incident intensity $I(t, \lambda)$ and absorption coefficient of the structure $A(\lambda)$. Penetration of laser radiation into metal and its absorption lead to the spatially distributed generation of the heat with a density F(x, t) described by

$$F(x,t) = A(\lambda)I(t)\frac{\alpha(x,\lambda)|E(x)|^2}{\int \alpha(x,\lambda)|E(x)|^2 dx}, \tag{5}$$

where $\alpha(x, \lambda)$ is the light absorption coefficient for the wavelength λ at specific point of the structure x. The profile of the $F(x, t)$ is shown in Fig. 2(a) by the red line. Temporal variation of the temperature profile within the structure can be found by solving inhomogeneous heat equation:

$$c\rho\frac{dT}{dt} = \frac{d}{dx}\left(\kappa\frac{dT}{dx}\right) + F(x,t), \tag{6}$$

where c is a specific heat capacity, κ is the thermal conductivity, ρ is the density. Sometimes it is suitable to use homogeneous heat equation in the form

$$\frac{dT}{dt} = D\frac{d^2T}{dx^2}, \tag{7}$$

Optics EXPRESS

where $D = \kappa/(c\rho)$ is the thermal diffusivity. Performance of the PAG-TP is defined by the dynamics of the temperature distribution, and for a quantitative understanding of the temperature relaxation processes, we first consider heating of the structure by an infinitely short laser pulse with energy density G. Since the materials of Bragg reflector adjacent to the metal do not absorb light, the short single laser pulse is absorbed only in the metal layer, leading to the formation of temperature profile defined by product $\alpha(x)|E(x)|^2$ shown in Fig. 2(a). In the subsequent modeling we assume that PAG-TP is confined from the both sides by the heat sinks supporting room temperature. After the end of the heating laser pulse the structure starts to cool. We can estimate the characteristic time of the temperature relaxation in the structure using well known relation

$$x^2 = 2Dt \tag{8}$$

The thermal diffusivity of the metals is more than one order of magnitude larger than for $Si0_2$ and TiO_2. Thus, according to Eq.(5), the temperature relaxation within the metal will occur much faster than in the BR. During the initial stage of cooling, the temperature decreases by factor of two in the time $\tau_1 = \frac{\xi^2}{2D_M}$, which is 3 ps for the structure under study. Then, the temporal dependence of the temperature increase, ΔT, in the sample is governed by the fundamental solution for the thermal conductivity equation, requiring that

$$\Delta T \sim \sqrt{1/t} \tag{9}$$

and then homogeneous temperature distribution within the metal layer occurs approximately within a characteristic time $\tau_2 = \frac{d_M^2}{2D_M}$. For the thickness of metal d_M =1 μm, the spreading of heat within the metallic layer occurs within ~7 ns. Figure 3(a) shows the temporal evolution of the temperature profile in the structure obtained by the numerical solving of Eq. (7) after heating by an infinitely sort laser pulse with energy density $G = 1$ mJ/cm^2 . Inhomogeneous and homogeneous heat Eqs. (6) and (7) were solved numerically using the finite difference methods [29]. The initial distribution of temperature profile repeats the profile of heat density $F(x)$. Then, the temperature reduces according to Eq. (9), and the profile is spreading; ΔT decreases by a factor of two during 2 ps, while the leveling of the temperature in the metallic layer occurs within 1 ns. Note that most of the heat goes into the metal, but only a small part of the BR (with thickness of ~ 100 nm) adjacent to the metal has a temperature comparable to those of the metal. Figure 3(b) shows the time variation of temperature distribution in the structure heated with a 10-ns laser pulse with sine slow amplitude and energy density $G = 10$ mJ/cm^2, in this case peak flux density is 2×10^6 W/cm^2 and maximum power density near the interface between the Bragg mirror and metal is 10^{12} W/cm^3. During the first half of the heating pulse, when the flux density of the pulse increases, the temperature profile has a maximum at the metal-BR interface. On the other hand, the temperature of the BR layers adjacent to the metal increases. After the end of the heating pulse, at 10 ns, the temperature peak shifts to the first BR layer. Thermal diffusivity of the BR materials is small; thus, the heat accumulated in the BR will slow down the temperature relaxation in the structure. Figure 4(a) shows the pattern of the profile $\Delta T(x, t)$ under periodic heating of the structure with a laser with modulation frequency 100 MHz and the time-average flux density $\overline{I(t)} = 10^6$ W/cm^2.

During the first pulse the temperature increases up to 80 °C, but subsequently the oscillation amplitude of ΔT for this case is about 40 °C: the temperature does not reduce fast enough. The variation of the structure surface position induced by thermal expansion reads as:

$$\Delta x = \int \varepsilon \Delta T(x) dx. \tag{10}$$

Figure 5(a) shows that the shift of the surface by almost 1 nm at the first period of excitation followed by a sinusoidal oscillation with a magnitude of ~0.5 nm accompanied by a constant

Optics EXPRESS

shift of the surface about 0.8 nm due to the heating of the structure as a whole. The constant shift of the surface during few subsequent pulses slightly increases and after 100 ns its temporal dependence tends to fixed value.

Note that for the parameters considered and the structure placed into a water-like medium the sound flux density is about 2 W/cm^2 in CW mode and corresponding pressure of the acoustic wave, obtained by Eq. (3) is about 1 MPa.

It was reported that for other types of photoacoustic emitters, the laser fluxes of the order 10 MW/cm^2 induce acoustic waves with pressure of the order of 10 MPa [30,31,32]. Thus, operational regime used for our structure does not approach conditions, leading to optical or mechanical destruction of the structures.

Since the power of sound emitted by the oscillating surface, defined by Eq.(2), is proportional to the magnitude of oscillation squared, it would be advantageous to provide the cool-down of the structure to the initial level after the end of the heating pulse, which can be achieved by the reduction of the repetition rate. In Fig. 4(b), the pattern of $\Delta T(x, t)$, i.e. the sequence of heating

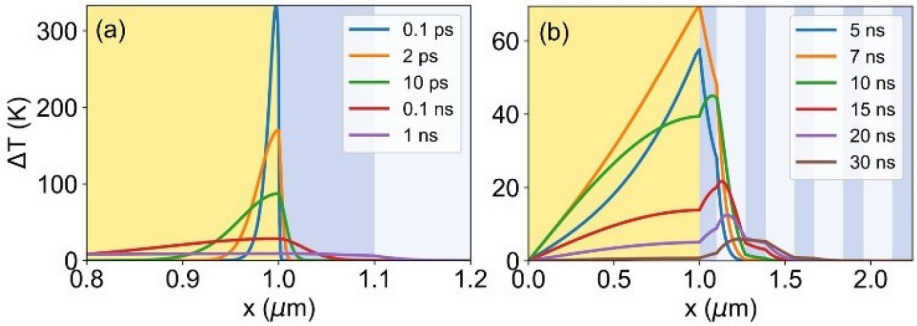

Fig. 3. Modification of the spatial profile of the temperature in the structure after heating by a single laser pulse with heating density profile shown in Fig. 2(a), for infinitely short pulse with energy density 1 mJ/cm^2 (a) and pulse of sinusoidal shape with duration 10 ns (b) and energy 10 mJ/cm^2. Results are obtained by solving Eqs. (6) and (7).

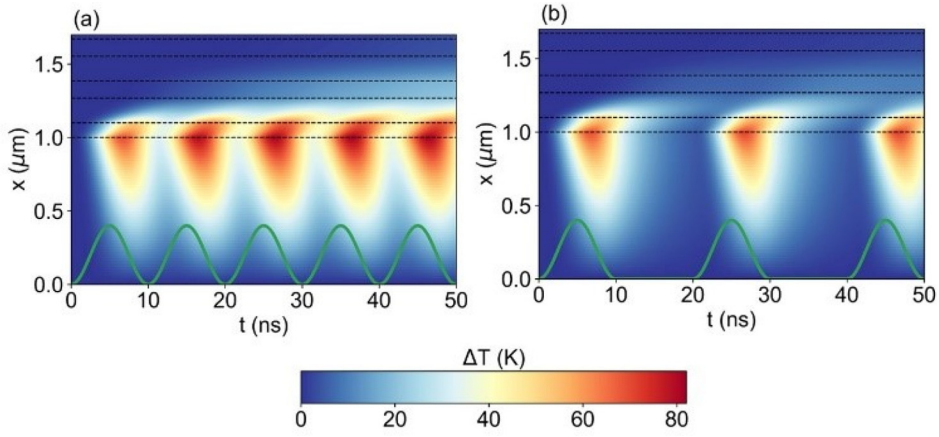

Fig. 4. Temporal and spatial distribution of the temperature increase $\Delta T(x, t)$ under periodic heating of the structure (a) with modulation of laser power at frequency of 100 MHz and average flux density $\overline{I(t)} = 10^6$ W/cm^2; (b) with a sequence of sinusoidal pulses with duration of 10 ns and repletion rate 50 MHz, and average flux density $\overline{I(t)} = 5*10^5$ W/cm^2. Green lines show the temporal dependence of laser flux density I(t).

Optics EXPRESS

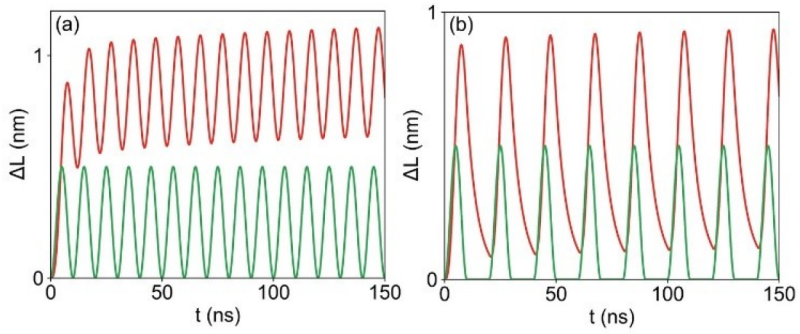

Fig. 5. Oscillation of the surface of the structure during heating by a laser (a) with sinusoidal modulation of the laser power $I(t)$ with frequency 100 MHz, and time-average flux density $\overline{I(t)}$ = 10^6 W/cm^2, (b) with a sequence of sinusoidal pulses with duration of 10 ns and repletion rate 50 MHz, and time-average flux density $\overline{I(t)}$ = 5*10^5 W/cm^2. Green lines show the temporal dependence of laser flux density I(t).

pulses with repetition rate of 50 MHz, is shown by the green line. In this case the structure cools down to the initial level between pulses and the magnitude of the surface oscillation increases up to 0.9 nm, as shown in Fig. 5(b).

4. Summary

The novel scheme of a photoacoustic generator based on the TP structure has been proposed. The TP structure provides a total absorption of the laser pulse at any desirable wavelength allowing the use of compact, powerful and feasible infrared semiconductor lasers with the wavelength about 1 μm for photoacoustic generators. Performance of various materials has been analyzed and it was shown that the structure utilizing magnesium for the active element possesses maximal efficiency. We have found that the power efficiency of light-to-sound conversion for the case considered reaches the value up to 10^{-5}.

Different schemes of photoacoustic emitters demonstrate conversion efficiencies, varying by many orders of magnitude. Bare metallic film demonstrates conversion efficiency of the order of 1 from 10^{-8} [33]. The media, providing enhanced absorption light, like graphene, carbon nanotubes or metal nanoparticles demonstrates efficiency of the order of 10^{-5} [9,34,35]. The highest efficiency, of the order of 10^{-3}, is demonstrated by composite made of polydimethylsiloxane (possessing extremely high thermal expansion coefficient) and gold nanoparticles (responsible for the absorption of light) [36]. The scheme proposed in our paper can combine the use of organic materials, possessing high thermal expiation coefficient, and advantages of thin film technologies, leading to even higher conversion efficiencies. The reported results provide a background for development of a new feasible and efficient type of photo-acoustic devices.

Funding

Belarusian Republican Foundation for Fundamental Research (F19RM-006); Energimyndigheten (# 46563-1); Vetenskapsrådet (#2019-05154); Russian Foundation for Basic Research (19-52-04005).

Disclosures

The authors declare no conflicts of interest.

Optics EXPRESS

See Supplement 1 for supporting content.

References

1. C. Hu, Z. Yu, and A. Wang, "All fiber-optic multi-parameter structure health monitoring system," Opt. Express **24**(18), 20287–20296 (2016).
2. S. D. Sharples, M. Clark, and M. G. Somekh, "Spatially resolved acoustic spectroscopy for fast noncontact imaging of material microstructure," Opt. Express **14**(22), 10435–10440 (2006).
3. T. Buma, M. Spisar, and M. O'Donnell, "A high-frequency, 2-D array element using thermoelastic expansion in PDMS," IEEE Trans. Ultrason. Ferroelectr. Freq. Control **50**(9), 1161–1176 (2003).
4. A. Baerwald, S. Dauk, R. Kanthan, and J. Singh, "Use of ultrasound biomicroscopy to image human ovaries in vitro," Ultrasound Obstet. Gynecol. **34**(2), 201–207 (2009).
5. V. V. Kozhushko and P. Hess, "Nondestructive evaluation of microcracks by laser-induced focused ultrasound," Appl. Phys. Lett. **91**(22), 224107 (2007).
6. Y. Hou, J.-S. Kim, S. Ashkenazi, M. O'Donnell, and L. J. Guo, "Optical generation of high frequency ultrasound using two-dimensional gold nanostructure," Appl. Phys. Lett. **89**(9), 093901 (2006).
7. N. Wu, Y. Tian, X. Zou, V. Silva, A. Chery, and X. Wang, "High-efficiency optical ultrasound generation using one-pot synthesized polydimethylsiloxane-gold nanoparticle nanocomposite," J. Opt. Soc. Am. B **29**(8), 2016–2020 (2012).
8. X. Zou, N. Wu, Y. Tian, and X. Wang, "Broadband miniature fiber optic ultrasound generator," Opt. Express **22**(15), 18119–18127 (2014).
9. Y. Hou, J.-S. Kim, S.-W. Huang, L. S. Ashkenazi, J. Guo, and M. O'Donnell, "Characterization of a broadband all-optical ultrasound transducer– from optical and acoustical properties to imaging," IEEE Trans. Ultrason. Ferroelectr. Freq. Control **55**(8), 1867–1877 (2008).
10. A. P. Mikitchuk and K. V. Kozadaev, "Simulation of the optical properties of surface nanostructures for photoacoustic converters," Quantum Electron. **48**(7), 630–636 (2018).
11. X. Ma, B. Liu, Y. Cai, D. Jia, B. Fu, and J. Ma, "Suppression of reverberations at fiber tips for optical ultrasound sensing," Opt. Lett. **45**(9), 2526–2529 (2020).
12. T. Goto, A. V. Dorofeenko, A. M. Merzlikin, A. V. Baryshev, A. P. Vinogradov, M. Inoue, A. A. Lisyansky, and A. B. Granovsky, "Optical Tamm states in one-dimensional magnetophotonic structures," Phys. Rev. Lett. **101**(11), 113902 (2008).
13. M. E. Sasin, R. P. Seisyan, M. A. Kalitteevski, S. Brand, R. A. Abram, J. M. Chamberlain, A. Y. Egorov, A. P. Vasil'ev, V. S. Mikhrin, and A. V. Kavokin, "Tamm plasmon-polaritons: slow and spatially compact light," Appl. Phys. Lett. **92**(25), 251112 (2008).
14. C. Symonds, G. Lheureux, J. P. Hugonin, J. J. Greffet, J. Laverdant, G. Brucoli, A. Lemaitre, P. Senellart, and J. Bellessa, "Confined Tamm plasmon lasers," Nano Lett. **13**(7), 3179–3184 (2013).
15. R. Brückner, A. A. Zakhidov, R. Scholz, M. Sudzius, S. I. Hintschich, H. Fröb, V. G. Lyssenko, and K. Leo, "Phase-locked coherent modes in a patterned metal-organic microcavity," Nat. Photonics **6**(5), 322–326 (2012).
16. M. A. Kaliteevski, A. A. Lazarenko, N. D. Il'inskaya, Y. M. Zadiranov, M. E. Sasin, D. Zaitsev, V. A. Mazlin, P. N. Brunkov, S. I. Pavlov, and A. Y. Egorov, "Experimental Demonstration of Reduced Light Absorption by Intracavity Metallic Layers in Tamm Plasmon-based Microcavity," Plasmonics **10**(2), 281–284 (2015).
17. K. Kamath, J. Phillips, H. Jiang, J. Singh, and P. Bhattacharya, "Small-signal modulation and differential gain of single-mode self-organized quantum dot lasers," Appl. Phys. Lett. **70**(22), 2952–2953 (1997).
18. L. J. Mawst, A. Bhattacharya, J. Lopez, D. Botez, D. Z. Garbuzov, L. DeMarco, J. C. Connolly, M. Jansen, F. Fang, and R. F. Nabiev, "8 W continuous wave front-facet power from broad-waveguide Al-free 980 nm diode lasers," Appl. Phys. Lett. **69**(11), 1532–1534 (1996).
19. A.D. Pierce, "Acoustics. An Introduction to Its Physical Principles and Applications," 3rd ed. (Springer, 2019).
20. E. Welsch, K. Ettrich, D. Ristau, and U. Willamowski, "Absolute Measurement of Thermophysical and Optical Thin-Film Properties by Photothermal Methods for the Investigation of Laser Damage," Int. J. Thermophysics **20**(3), 965–976 (1999).
21. R. A. Serway and J.W. Jewett, "Physics for Scientists and Engineers," 9th ed. (Cengage Learning, 2010), Chap. 17, p. 439.
22. L. E. Kinsler, A. R. Frey, A. B. Coppens, and J. V. Sanders, "Fundamentals of acoustics," 4th ed. (Wiley, 1999). p. 124.
23. D. Crooks, C. Gianpietro, M. M. Fejer, G. Harry, J. Hough, P. T. Khuri-Yakub, S. Penn, R. Route, S. Rowan, P. H. Sneddon, I. O. Wygant, and G. G. Yaralioglu, "Experimental measurements of mechanical dissipation associated with dielectric coatings formed using SiO_2, Ta_2O_5 and Al_2O_3," Class. Quantum Grav. **23**(15), 4953–4965 (2006).
24. C.-L. Tien, C.-C. Jaing, C.-C. Lee, and K.-P. Chuang, "Simultaneous determination of the thermal expansion coefficient and the elastic modulus of Ta_2O_5 thin film using phase shifting interferometry," J. Modern Opt. **47**(10), 1681–1691 (2000).
25. V. B. Braginsky and A. A. Samoilenko, "Measurements of the optical mirror coating properties," Phys. Lett. A **315**(3-4), 175–177 (2003).

Optics EXPRESS

26. W. Zhu, G. Zheng, S. Cao, and H. He, "Thermal conductivity of amorphous SiO_2 thin film: A molecular dynamics study," Sci. Rep. **8**(1), 10537 (2018).
27. J. W. Arblaster, "Selected values of the crystallographic properties of the elements," (ASM International, 2018), p. 573W.
28. G. Pozina, M. A. Kaliteevski, E. V. Nikitina, D. V. Denisov, N. K. Polyakov, E. V. Pirogov, L. I. Goray, A. R. Gubaydullin, K. A. Ivanov, N. A. Kaliteevskaya, A. Y. Egorov, and S. J. Clark, "Super-radiant mode in InAs-monolayer–based Bragg structures," Sci. Rep. **5**(1), 14911 (2015).
29. M. Necati Özişik, Helcio R. B. Orlande, Marcelo J. Colaço, and Renato M. Cotta, "Finite Difference Methods in Heat Transfer," 2nd ed. (Taylor and Francis Group, 2017), p. 129.
30. S. Noimark, R. J. Colchester, B. J. Blackburn, E. Z. Zhang, E. J. Alles, S. Ourselin, P. C. Beard, I. Papakonstantinou, I. P. Parkin, and A. E. Desjardins, "Carbon-Nanotube-PDMS Composite Coatings on Optical Fibers for All-Optical Ultrasound Imaging," Adv. Funct. Mater. **26**(46), 8390–8396 (2016).
31. S. Hwan Lee, M. Park, J. J. Yoh, H. Song, E. Yun Jang, Y. Hyup Kim, S. Kang, and Y. Seop Yoon, "Reduced graphene oxide coated thin aluminum film as an optoacoustic transmitter for high pressure and high frequency ultrasound generation," Appl. Phys. Lett. **101**(24), 241909 (2012).
32. R. J. Colchester, C. A. Mosse, D. S. Bhachu, J. C. Bear, C. J. Carmalt, I. P. Parkin, B. E. Treeby, I. Papakonstantinou, and A. E. Desjardins, "Laser-generated ultrasound with optical fibres using functionalised carbon nanotube composite coatings," Appl. Phys. Lett. **104**(17), 173502 (2014).
33. E. Biagi, F. Margheri, and D. Menichelli, "Efficient laser-ultrasound generation by using heavily absorbing films as targets," IEEE Trans. Ultrason., Ferroelect., Freq. Contr. **48**(6), 1669–1680 (2001).
34. T. Lee, H. W. Baac, Q. Li, and L. J. Guo, "Efficient Photoacoustic Conversion in Optical Nanomaterials and Composites," Adv. Opt. Mater. **6**(24), 1800491 (2018).
35. H. W. Baac, J. G. Ok, A. Maxwell, K.-T. Lee, Y.-C. Chen, A. J. Hart, Z. Xu, E. Yoon, and L. J. Guo, "Carbon nanotube optoacoustic lens for focused ultrasound generation and high-precision targeted therapy," Sci. Rep. **2**(1), 989 (2012).
36. X. Zou, N. Wu, Y. Tian, and X. Wang, "Broadband miniature fiber optic ultrasound generator," Opt. Express **22**(15), 18119 (2014).